AIR FORCE INST OF TECH WRIGHT-PATTERSON AFB OHIO SCH--ETC F/G 11/6
ABSORPTANCE OF IR LASER RADIATION AT A METALLIC INTERFACE AT VA--ETC(U)
DEC 77 R A HENSON

UNCLASSIFIED AFIT/GEP/PH/77-5

NL

| OF |
AD
A055256

END
DATE
FILMED

7 -78

DDC

1

6 ABSORPTANCE OF IR LASER RADIATION AT A
METALLIC INTERFACE AT VARIOUS ANGLES OF
INCIDENCE AND POLARIZATIONS.

9 Master's THESIS,

14 AFIT/GEP/PH/77-5   10 Richard A. Henson
Captain   USAF

D D C
RECEIVED
JUN 19 1978
E

11 Dec 77   13 65p.

18 06 13 085

012 225 mt

ABSORBTANCE OF IR LASER RADIATION AT A METALLIC INTERFACE
AT VARIOUS ANGLES OF INCIDENCE AND POLARIZATIONS

THESIS

Presented to the Faculty of the School of Engineering

of the Air Force Institute of Technology

Air University

in Partial Fulfillment of the

Requirements for the Degree of

Master of Science

by

Richard A. Henson, B.S.
Captain   USAF

Graduate Engineering Physics

December 1977

Preface

This thesis has been an effort to examine the absorptance of laser radiation at a metallic interface. The absorptance has been examined at various angles of incidence and laser beam polarizations. I have thoroughly enjoyed the work and feel I have gained great insight into how to approach a problem.

I would like to express my appreciation to my advisor, Captain Allen M. Hunter, Air Force Institute of Technology, for his guidance and understanding. His advice was a major contribution to the completion of this thesis.

I am also grateful to James E. Hitchcock, Air Force Institute of Technology, for his recommendations. My thanks to Captain John Campbell, Aeronautical Systems Division, and Mr. Jim Weaver, Air Force Materials Laboratory, for sponsoring the thesis. I would like to thank the physics laboratory technicians for their cooperation and assistance.

Finally, I would like to express my appreciation to my wife, Ellen, for her understanding, support, and encouragement.

TABLE OF CONTENTS

TABLES OF CONTENTS (Cont'd)

LIST OF FIGURES

LIST OF TABLES

List of Symbols

a   Major axis dimension of an ellipse (cm)

α Absorptance

α_h Subscript h indicates parallel (horizontal) polarization

α_v Subscript v indicates perpendicular (vertical) polarization

α_u Subscript u indicates random polarization

A   Surface area (cm^2)

A_c Subscript c denotes for Cu

A_a Subscript a denotes for Al

A_T Subscript T denotes for Ti

b   Minor axis dimension of an ellipse (cm)

C   Specific heat ($\frac{cal}{g\ ^\circ C}$)

ϵ Total emissivity

g $1 - \frac{L}{R}$ ('g' parameter) (R = mirror radius of curvature)

h   Convection coefficient ($\frac{cal}{s\ cm\ ^\circ C}$)

k   Thermal conductivity ($\frac{cal}{s\ cm^2\ ^\circ C}$)

k_2 Extinction coefficient of a metal

κ Diffusivity ($\frac{cm}{s}$)

L   CO laser cavity length (cm)

λ Wavelength (μm)

$\tilde{n}$ Complex index of refraction

n   Index of refraction

P   Power ($\frac{cal}{s}$)

P_i Incident power

P_r Reflected power

P_t Total power without the Brewster's window

r Radius (cm)

R Reflectance

R_1 Radius of curvature of a laser mirror (cm)

ρ Density $(\frac{g}{cm^2})$

σ Stefan-Boltzman number $(\frac{cal}{s\ cm^2\ (°K)^4})$

σ_1 Stefan-Boltzman number for the small temperature approximation

t Time (s)

T Temperature (°K)

T_a Ambient temperature (°K)

$\frac{dT}{dt}$ The net rate of temperature increase in the sample $(\frac{°K}{s})$

θ_1 The angle of incidence as measured from the normal

V Volume (cm³)

W_0 The waist of the CO beam (1/e point) (cm)

$W(z_1)$ The 1/e point radius of the beam at a distance z (cm)

z_1 The distance from the waist (cm)

z Thickness of metal (Al, Cu, or Ti) (cm)

ABSTRACT

A calorimetric method is developed to measure the absorptance of IR laser radiation at a metallic interface. The absorptance of Al and Ti is measured at various angles of incidence (10° - 87°) and laser polarizations (parallel, perpendicular, and random relative to the plane of incidence). Designing the metal surface to be approximately the size of the beam and using a thin (0.032 in) sample facilitate the simplifying assumptions. The average incident power is 13 w/cm^2. For the laser polarizations, parallel and perpendicular, the maximum difference between theoretically and experimentally calculated values is 26 percent and 57 percent respectively for Al and 100 percent and 500 percent respectively for Ti. The Ti values are largely attributed to surface roughness (sanded) and oxidation. Without a Brewster window in the laser cavity, a test revealed the laser polarization was not 50 percent horizontal and 50 percent vertical. The average polarization is 17 percent horizontal and 83 percent vertical.

ABSORPTANCE OF IR LASER RADIATION AT A METALLIC INTERFACE
AT VARIOUS ANGLES OF INCIDENCE AND POLARIZATIONS

I. INTRODUCTION

Background

The absorptance (α) of laser radiation at a metallic interface has been predicted for many years by the Fresnel equations in Reference 1. The absorptance is predicted as a function of the angle of incidence (θ_1) and the index of refraction for various incident radiation polarizations. Theoretical calculations for randomly polarized light normally assume 50 percent parallel and 50 percent perpendicular polarizations (relative to the plane of incidence).

Recent tests assuming a random polarization of incident radiation have indicated the absorptance calculated may vary from theoretically calculated values by as much as a factor of three (Ref 2:personal correspondence) at $\theta_1 = 80°$ from the normal. The results were based on the metal burn-through time. At $\theta_1 = 10°$, the calculated absorptance was approximately 1.4 times greater than the theoretical values (Ref 2: personal correspondence). The above tests were accomplished at high power densities (15 kw/cm^2) on unpainted 2024 aluminum clad metal (0.032 in. thick).

Present Study

The purpose of this study is to measure the absorptance at various angles of incidence (θ_1) and at various laser beam polarizations. The absorptance is measured for a polished aluminum surface and for a sanded

titanium surface. The angle of incidence as measured from the normal is varied from 10 degrees to 87 degrees. The absorptance is measured for three laser beam polarizations: parallel, perpendicular, and unpolarized relative to the plane of incidence. A calorimetric method is utilized to determine the absorptance (α).

For the readers convenience, the Fresnel equations (Ref 1:628-633) are presented to facilitate the comparison of existing theoretical values and the experimental values of α.

The proposed calorimetric method assumes the temperature in the metal is independent of position. Evaporating the Al or Ti onto a Cu substrate reduces the spatial variation by increasing the thermal conductivity of the metal. The metal surface area is designed to conform to the cross sectional laser beam area to facilitate uniform irradiation of the metal surface.

The experimental apparatus and procedure simply involve irradiating a small metal surface, measuring the incident power, and recording the temperature increase in the metal sample.

For Al, the difference between theory and experimental values varies as much as 57 percent over all θ_1 and polarizations. For Ti, these differences vary from 100 percent to 500 percent. Such differences may be attributed to surface conditions (roughness and oxidation).

Finally, the degree of polarization for the unpolarized laser beam is determined. The test indicates the assumption of 50/50 polarization is not valid.

II. THEORY

Fresnel Equations

When light is incident upon a planar metallic interface, the light is absorbed, reflected, and transmitted (thin films). If the metal is thicker than the skin depth, no light will be transmitted. Therefore,

$$\alpha = 1 - R \tag{1}$$

where, α is the absorptance and R is the reflectance. The reflectance is predicted by the Fresnel equations (Ref 1:629) as a function of the angle of incidence and the index of refraction. For the laser beam polarization perpendicular to the plane of incidence, the reflectance (R_v) is (Ref 1:629):

$$R_v = \frac{(n_1 \cos\theta_1 - u_2)^2 + v_2^2}{(n_1 \cos\theta_1 + u_2)^2 + v_2^2} \tag{2}$$

For the polarization parallel, the reflectance (R_h) is (Ref 1:629):

$$R_h = \frac{[n_2^2(1-k_2^2) \cos\theta_1 - n_1 u_2]^2 + [2n_2^2 k_2 \cos\theta_1 - n_1 v_2]^2}{[n_2^2(1-k_2^2) \cos\theta_1 + n_1 u_2]^2 + [2n_2^2 k_2 \cos\theta_1 + n_1 v_2]^2} \tag{3}$$

where, the complex index of refraction of the metal takes the form:

$$\tilde{n}_2 = n_2(1+ik_2) \tag{4}$$

θ_1 is the angle of incidence as measured from the normal and n_1 is the index of refraction of air. The values of u_2 and v_2 are determined from (Ref 1:628):

3

$$2u_2^2 = n_2^2(1-k_2^2) - n_1^2\sin^2\theta_1 + \{[n_2^2(1-k_2^2) - n_1^2\sin^2\theta_1]^2 + 4n_2^4k_2^2\}^{\frac{1}{2}} \qquad (5)$$

$$2v_2^2 = -[n_2^2(1-k_2^2) - n_1^2\sin^2\theta_1] + \{[n_2^2(1-k_2^2) - n_1^2\sin^2\theta_1]^2 + 4n_2^4k_2^2\}^{\frac{1}{2}} \qquad (6)$$

For random polarization, the absorptance (α_u) is determined by:

$$\alpha_u = \frac{\alpha_v + \alpha_h}{2} \qquad (7)$$

The theoretical values are listed in Appendix C for Al and Ti using the constants in Appendix E. Calculations for an Air/Al_2O_3/Al interface are in Appendix C using the equations from Reference 1, page 633. Two assumptions are used in the later calculations. The Al_2O_3 is assumed to be 50Å thick and the imaginary part of the index of refraction (1.76+.1i) is neglected since the layer of Al_2O_3 is soo thin (Ref 3:344)

Calorimetric Theory for Calculations

In order to determine the absorptance by calorimetry, one must first solve the heat transfer equation. Using cylindrical coordinates, the temperature distribution in the metal is (Ref 4:17):

$$\frac{\partial T}{\partial t} = \kappa\left[\frac{\partial^2 T}{\partial r^2} + \frac{1}{r}\frac{\partial T}{\partial r} + \frac{1}{r^2}\frac{\partial^2 T}{\partial \theta^2} + \frac{\partial^2 T}{\partial z^2}\right] \qquad (8)$$

$$\kappa = \frac{k}{\rho C} = \text{diffusivity} \qquad (9)$$

k = thermal conductivity

ρ = density

and $\qquad C$ = specific heat

The solution to equation (8) may be simplified by assuming the temperature in the metal sample is approximately constant. The rate of energy increase in the

4

sample is equivalent to the power absorbed less the losses to convection and radiation. Mathematically (Ref 5:personal communication),

$$(\rho VC)\,\frac{dT}{dt} = \alpha P - hA(T-T_a) - \varepsilon A\sigma(T^4-T_a^4) \tag{10}$$

If we assume a small temperature change, equation (9) may be expressed as

$$(\rho VC)\,\frac{dT}{dt} = \alpha P - [hA+\varepsilon A\sigma_1 T_a^3]\,(T-T_a) \tag{11}$$

where

$\quad V$ = the sample volume

$\quad P$ = the incident power

$\quad h$ = the convection coefficient

$\quad A$ = the total sample surface area

$\quad T$ = the maximum temperature of the sample

$\quad T_a$ = the ambient temperature

$\quad \varepsilon$ = the total emissivity of the sample

$\quad \sigma_1$ = the Stephan-Boltzman number (altered)($\sigma_1 = 4\sigma$)

$\quad T_a^3$ = the ambient temperature in ($^\circ K)^3$

and $\quad (\rho VC)\,\frac{dT}{dt}$ = the total rate of increase of energy in the sample. The time history of the sample temperature will consist of a positive (exposed to the laser) slope and a negative (cooling) slope. For an example, see Appendix G. The negative slope is due to convection and radiation. These two terms dissipate heat during the positive slope portion also. Therefore, to determine $\frac{dT}{dt}$, one must add the absolute values of the positive and negative slopes. Equation (11) is valid as long as ΔT is not too large ($\Delta T \simeq 2^\circ C$).

5

In order to facilitate the isothermal approximation, the size and form of the metal surface area are designed the same as the laser beam cross sectional area. For example, at $\theta_1 = 0°$, the metal surface should be circular. At $\theta_1 = 60°$, the metal surface should be elliptical. The dimensions depend upon the spot size of the beam. The following equations are used to determine the spot size (Ref 6:308,324):

$$w_0 = \left(\frac{L\lambda}{\pi}\right)^{\frac{1}{2}} \left(\frac{g}{1-g}\right)^{\frac{1}{4}} \tag{12}$$

$$w(z_1) = w_0 \left[1 + \left(\frac{\lambda z_1}{\pi w_0^2}\right)^2\right]^{\frac{1}{2}} \tag{13}$$

$$g = 1 - \frac{L}{R_1} \tag{14}$$

where w = the radius at the 1/e power point

L = the cavity length

λ = the lasing wavelength

R_1 = the radius of curvature of the half symmetric laser resonator

and $w(z_1)$ is the spot size at a distance z_1 from w_0. For a Gaussian beam profile, 86 percent of the total power is within a radius of $w(z_1)$ and 99 percent within a radius of $1.5 w(z_1)$ (Ref 5:313). When the Brewster's window is mounted in the laser cavity, the cavity length is increased and therefore, the spot size is increased. For the laser used, $R_1 = 10m$, L = 1.35m, and $\lambda = 10.6\mu m$, $w_0 = 3.4 \times 10^{-3}m$. If $z_1 = 1m$, $w(1) = 4 \times 10^{-3}m$. The ellipse dimensions (major axis a and minor axis b) should be based on $1.5w(1)$ or $6 \times 10^{-3}m$. The minor axis dimension (b) is $6 \times 10^{-3}m$. For $\theta_1 = 70°$, the major axis dimension (a) is $\frac{w(1)}{\cos\theta_1}$ or $1.75 \times 10^{-2}m$. The isothermal approximation assumes the beam distribution

6

is uniform, not Gaussian. For a nonuniform beam, a hot spot will induce
a significant temperature variation in the sample.

To check the validity of the isothermal approximation, one can
check the time required for the temperature to penetrate the thickness
(z) of the sample. If z is small, and the temperature change is small,
the one dimensional heat equation is approximately (Ref 7:Personal
communication):

$$\frac{T}{t} \simeq \frac{\kappa T}{z^2} \tag{15}$$

therefore,

$$t \simeq \frac{z^2}{\kappa} \tag{16}$$

Using equation (9) and the values in Appendix E for Al and Cu, if
z = 0.0813 cm,

$$t_A \simeq 7 \times 10^{-3} s$$

$$t_C \simeq 6 \times 10^{-3} s$$

Therefore, the axial flow of heat is rapid and the isothermal approxima-
tion should hold for exposure times much greater than t_C.

The radial flow can be checked in a similar fashion with the following
approximation to the heat equation (Ref 7:Personal communication):

$$\frac{T}{t} \simeq \frac{\kappa T}{2r^2} \tag{17}$$

therefore,

$$t \simeq \frac{2r^2}{\kappa} \tag{18}$$

7

where r is the radius of the sample. This assumes only small radial changes in the temperature. Using equation (18) and the values for Al and Cu in Appendix E, if $r = 1$ cm,

$$t_A \simeq 2 \text{ s}$$

$$t_C \simeq 1.7 \text{ s}$$

These values represent the maximum time for radial flow if the sample radius is 1cm greater than the spot size radius. If the sample were 0.5 cm greater than the spot size,

$$t_A \simeq 0.5 \text{ s}$$

$$t_C \simeq 0.4 \text{ s}$$

As the area of the beam approaches the surface area of the metal, r (Equation 18) approaches zero as does the radial time flow. The resulting time is much smaller than the time of exposure of the metal.

III. EXPERIMENTAL APPARATUS AND PROCEDURE

Experimental Arrangement

Figure 1 is a block/line diagram of the experimental arrangement. See Appendix H for a parts list. The HeNe laser is coaligned with the CO_2 laser with mirrors one and two for easy visual alignment of the system. Once the system is aligned, mirror one is removed with a laterally adjusting bench mount. Brick one is simply an on-off switch for the CO_2 laser. Any part of the system can be changed without turning the CO_2 laser off.

The CO_2 laser can be polarized by inserting a factory built Brewster's window in the resonator cavity. The beam exit mirror is moved which increases the length of the cavity. The window may be rotated to change the polarization from parallel to perpendicular to the plane of incidence.

The incident power is measured prior to the sample exposure with the power detector and meter. The power is recorded on the same graph as the temperature curve.

The sample is suspended between three plexiglass rods. The rods are notched at one end to facilitate mounting the samples. No parts of the rod extend beyond the front surface of the sample. There are no obstructions between the sample surface and the beam at high angles of incidence. The rods do not conduct any significant amount of heat from the sample due to their low thermal conductivity. The rods are supported by an aluminum ring which is mounted to a nodel bench slide with lateral and azimuthal
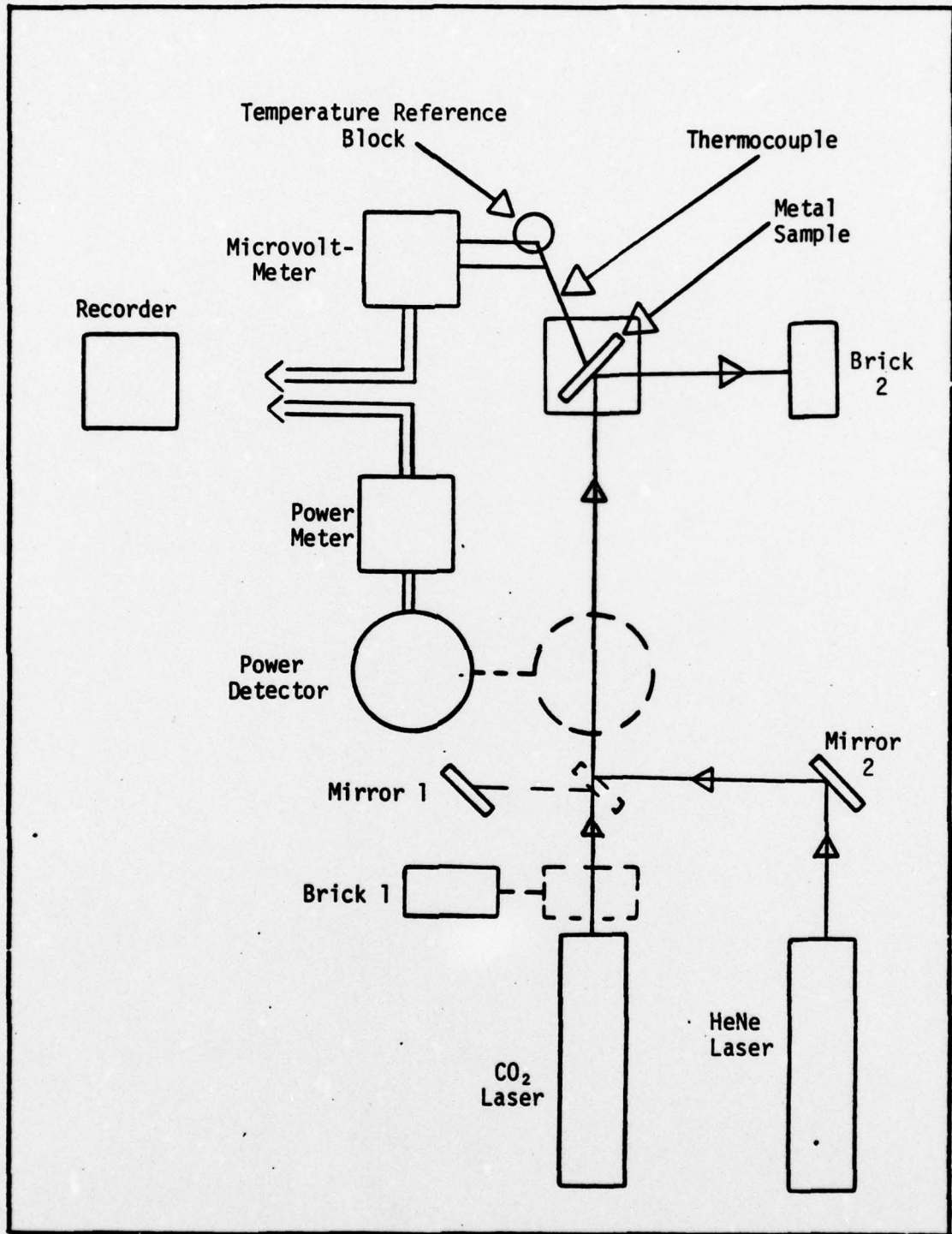
Figure 1. Experimental Diagram

10

adjustments. The metal sample is aligned normal to the HeNe beam by adjusting the reflected beam back upon the original beam. Angular adjustments about a horizontal axis (pitch) are reproducible within one degree and azimuthal adjustments are reproducible within one degree.

An Iron-Constantan thermocouple is used to measure the temperature rise of the sample. The thermocouple wire is supported through a plastic sleeve attached to a bench mount. The semi-rigid sleeve is used to force the thermocouple against the back of the sample with a small springlike force. Approximately 1/8 inch of the thermocouple is in contact with the sample. One side of the thermocouple leading from the sample proceeds via a metal temperature reference block and then on to the microvoltmeter. The other side proceeds directly to the micro-voltmeter. The thermocouple output is amplified with a microvoltmeter and then recorded. The recorder has a built-in time drive which enables one to record the temperature as a function of time.

Sample Description

Each sample consists of a 0.0813 cm copper substrate with approximately 400Å of evaporated Al or Ti. Six sample sizes were made for Al and six for Ti. One disc of radius 1.5 cm is used for $\theta_1 = 10°$ to $\theta_1 = 60°$. The other five samples are ellipses with the major (a) and minor (b) axes, and the appropriate angles of use presented in Table I. The samples will be referred to by number in increasing sizes.

11

TABLE I

Sample Dimensions and Angles of use

Sample Number	a(cm)	b(cm)	Primary angles of use (degrees)
1	1.54	0.52	60-70
2	2.28	0.54	70-80
3	3.09	0.52	80-83
4	4.19	1.03	83-85
5	7.05	1.03	85-87

The evaporation procedure for Al is in Appendix A and for Ti is in Appendix B.

The surface conditions of the Cu substrate determine the final surface condition after evaporation. The Cu substrate for the Al is wet sanded with 600A and 400A sand paper and then buffed with a polishing compound and a buffing wheel. The Cu substrate for the Ti is sanded with 600A and 4/0 sand paper and then hand buffed with a crocus cloth yielding a much rougher finish.

Experimental Procedure

This procedure assumes the HeNe laser is aligned as described previously and also assumes an understanding of the experimental apparatus (Table 1).

1. Brick one is placed to obstruct the CO_2 beam.

2. The CO_2 laser is turned on for a five minute warm up. Normally the laser is adjusted to 10μA current and 10mm of Hg pressure which yields approximately 10 watts of power. If polarization is required, the

Brewster window must be installed prior to turning on any power or pressure.

3. The sample is aligned using the HeNe laser and set at the desired angle. Brick two is positioned to absorb the reflected beam and the thermocouple is positioned at the back of the sample. Different thermocouple positions were utilized to check the temperature variations.

4. The power detector is aligned and the power meter is connected to the recorder. The desired instrument scales are selected (see Appendix D for calibrations).

5. Mirror one is removed.

6. The recorder time sweep is initiated and then brick one is removed. The incident power is normally recorded for 80 seconds.

7. Brick one is placed back in position. The microvoltmeter is connected to the recorder and the recorder is repositioned. The power meter is removed and at this point the sample is enclosed in a plexiglass box to reduce air currents.

8. The recorder time sweep is initiated and brick one is removed. The time of exposure was varied from three to 20 seconds, and then brick one is placed back in the system. The temperature is recorded for another 50 to 60 seconds to determine the heat losses.

9. A small fan is used to cool the sample back to room temperature prior to the next test. For retests, repeat steps three through eight.

13

Polarization Check

The degree of polarization of the laser is determined experimentally. The Brewster window is removed from the cavity and will be used external to the cavity for this check. Two terms are introduced to distinguish between the polarizations: horizontal polarization (P_H) and vertical polarization (P_V). The total power (P) without the Brewster's window is:

$$P = P_V + P_H \tag{20}$$

All the power polarized parallel to the plane of incidence is transmitted and 0.75 of the power polarized perpendicular is transmitted for the NaCl window at the Brewster's angle using n = 1.488 for NaCl at λ = 10.6μm.

The transmitted power is measured for the plane of the Brewster's window (at the Brewster angle) vertical. The Brewster window is rotated 90 degrees about the laser beam axis and the power is measured. Also, the power is measured without the window. The above tests were run twice (see Table II).

TABLE II

Power Versus Brewster Window Position

Test Number	Power (w)	Brewster Window Position		
		Vertical	Horizontal	Removed
1	3.17	x		
2	3.9		x	
3	3.95			x
4	3.3	x		
5	3.9		x	
6	4.0			x

14

For the window position vertical, the following equation will hold:

$$P_H + 0.75 \, P_V = P_t \qquad\qquad (21)$$

where, P_t is the transmitted (measured) power. For the horizontally positioned window, (at the Brewster angle),

$$0.75 \, P_H + P_V = P_t \qquad\qquad (22)$$

For the case of no window, $P_t = P$ in Equation (20). Any two of the equations may be solved to determine P_H and P_V. Six different sets of equations were solved, and the average P_H was 17 percent with minimum and maximum values of five percent and 30 percent respectively. All unpolarized laser beams are not polarized 50 percent parallel and 50 percent perpendicular to a given axis. This is not to say all lasers favor one polarization or even that this laser will yield the same results again.

15

IV. RESULTS AND DISCUSSIONS

This section will present a sample calculation, a table of results, a comparison of theoretical and experimental values, and an estimate of the relative error contributions to the heat equation.

Sample Calculation

For sample two, Al coated (400Å), 0.0813 cm Cu substrate, $\theta_1 = 40°$, a = 2.28 cm, b = 0.54 cm, and utilizaing the graph and constants in Appendices G and E respectively, the following calculation α_h is appropriate.

$$\alpha_h = \frac{1}{p} \{[(\rho VC)_C + (\rho VC)_A] \frac{dT}{dt} + [h(A_C+A_A) + \sigma_1 T_a^3 (\epsilon_C A_C + \epsilon_A A_A)](T-T_a)\} \tag{23}$$

The area of an ellipse is πab and the perimeter (p) is $4.4(a^2+b^2)^{\frac{1}{2}}$. Therefore,

$$V = \pi abz \tag{24}$$

and

$$A = \pi ab + pz \tag{25}$$

Using equations (23), (24), and (25),

$$\alpha_h = \frac{1}{p}[0.259 \frac{dT}{dt} + 7.13 \times 10^{-4}(T-T_a)]$$

where, T_a = 296°K. The following instrument scales were used:

Microvoltmeter = 300 V

Recorder Y   = 0.1 V/in

Recorder t   = 5 s/in

Power meter   = 30 w

Combining the calibrations in Appendix D and the constants in Appendix E, the conversions for the graph in Appendix G are:

Power Conversion $= \left(\dfrac{1W}{0.347V}\right)\left(0.2389\ \dfrac{cal/s}{W}\right)\left(0.102\ \dfrac{V}{in}\right) = 0.70\ \dfrac{cal/s}{in}$

Temperature Scale $\left(\dfrac{1^{\circ}C}{0.053mV}\right)\left(0.314\dfrac{mV}{V}\right)\left(0.102\ \dfrac{V}{in}\right) = 0.60\ \dfrac{^{\circ}C}{in}$

Therefore,

$$\alpha_H = \frac{1}{\left(0.70\ \dfrac{cal/s}{in}\right)\left(3.85\ in\right)}\left[0.259\left(0.60\ \dfrac{^{\circ}C}{in}\right)\left(0.2\dfrac{in}{s}\right)\left(2.26\right)\right.$$

$$\left. +\ 7.13 \times 10^{-4}\left(0.60\ \dfrac{^{\circ}C}{in}\right)\left(2.2\ in\right)\right]$$

$\alpha_H = 0.026$

This value agrees with the theory for $\theta_1 = 40^{\circ}$ as listed in Appendix C for Al.

Tables of Results

Table III is a summary of the average calculated values of α and of the mean deviation from the average for Al. Since the variation of the thermocouple position was inconclusive, the position will not be listed. The absorptance is listed at various θ_1 and polarizations.

Table IV is a similar summary for Ti.

TABLE III

Average Calculated Absorptance of Al and Mean Deviations from the Average

θ	10	20	30	40	50	60	70	80	83	85	87
α_H	.018 ±.001	.02 ±.003	.02 ±.003	.027 ±.006	.03 ±.005	.043 ±.007	.057 ±.007	.113 ±.019	.171 ±.027	.249 ±.308	.355 ±.068
α_V	.017 ±.002	.016 ±.001	.016 ±.002	.015 ±.002	.013 ±.002	.013 ±.001	.011 ±.002	.007 ±.003			
α_U	.017 ±.001	.016 ±.005	.019 ±.002	.019 ±.002	.014 ± 0	.02 ± 0	.026 ± 0	.026 ±.006	.022 ±.01	.069 ± 0	.076 ± 0

α_V was too small to measure accurately for $\theta_1 > 80°$

18

TABLE IV

Average Calculated Absorptance of Ti and the Mean Deviations from the Average

θ	10	20	30	40	50	60	70	80	83	85	87
α_H	.151	.194	.235	.302	.298	.335	.449	.536	.671	.729	.764
	±.027	±.01	±.012	±.037	±.006	±.012	±.008	±.051	±.101	±.018	± 0
α_V	.205	.173	.178	.162	.133	.107	.066	.058	.067	.032	.032
	± 0	±.003	±.002	± 0	±.005	±.01	±.002	±.026	±.02	±.002	±.005
α_U	.218	.217	.190	.166	.181	.161	.140	.132	.120	.141	.182
	±.001	±.011	±.003	±.005	±.016	±.023	±.014	±.015	±.04	±.037	±.002

Comparisons

Six graphs are utilized to facilitate trend comparisons of theoretical values with the experimental (calorimetric) values. All graphs have the theoretical curves for the bare metal as presented in Appendix C. The first three graphs are for Al in the following order of polarizations: α_H, α_V, and α_U. Similarly, three graphs are presented for Ti. The scale is the same for all graphs to facilitate comparisons between graphs.

The maximum difference between theoretical and experimental values in Figure 2 (α_H) is 26 percent at $\theta_1 = 85°$. The majority of the differences are less than 15 percent for $\theta_1 < 70°$. If we compare the experimental values to the theoretical values for an Air/Al_2O_3/Al interface (Appendix C), the maximum difference is 21 percent at $\theta_1 = 85°$. The majority of the other differences will be less than 10 percent for $\theta_1 < 70°$. The differences between the theoretical and experimental values are within experimental error.

In Figure 3, (α_V) has a maximum difference at $\theta_1 = 80°$ of 57 percent. The next largest difference is 33 percent at $\theta_1 = 70°$. Although the percent difference is large, at 80°, the absorptance is approaching the minimum measuring capacity of the experimental apparatus.

The theoretical values in Figure 4 (α_U) assume a 50/50 random polarization which has been shown to be in error. The experimental values of α_V and α_H may be used to find α_U for a 50/50 polarization.

Figures 5, 6, and 7 for Ti lend themselves to the same analogies as Al with a few exceptions. First, the theory assumes an optically

Figure 2. Absorptance of Al. Polarization Parallel to the Plane of Incidence.

21

Figure 3. Absorptance of Al. Polarization Perpendicular to the Plane of Incidence.

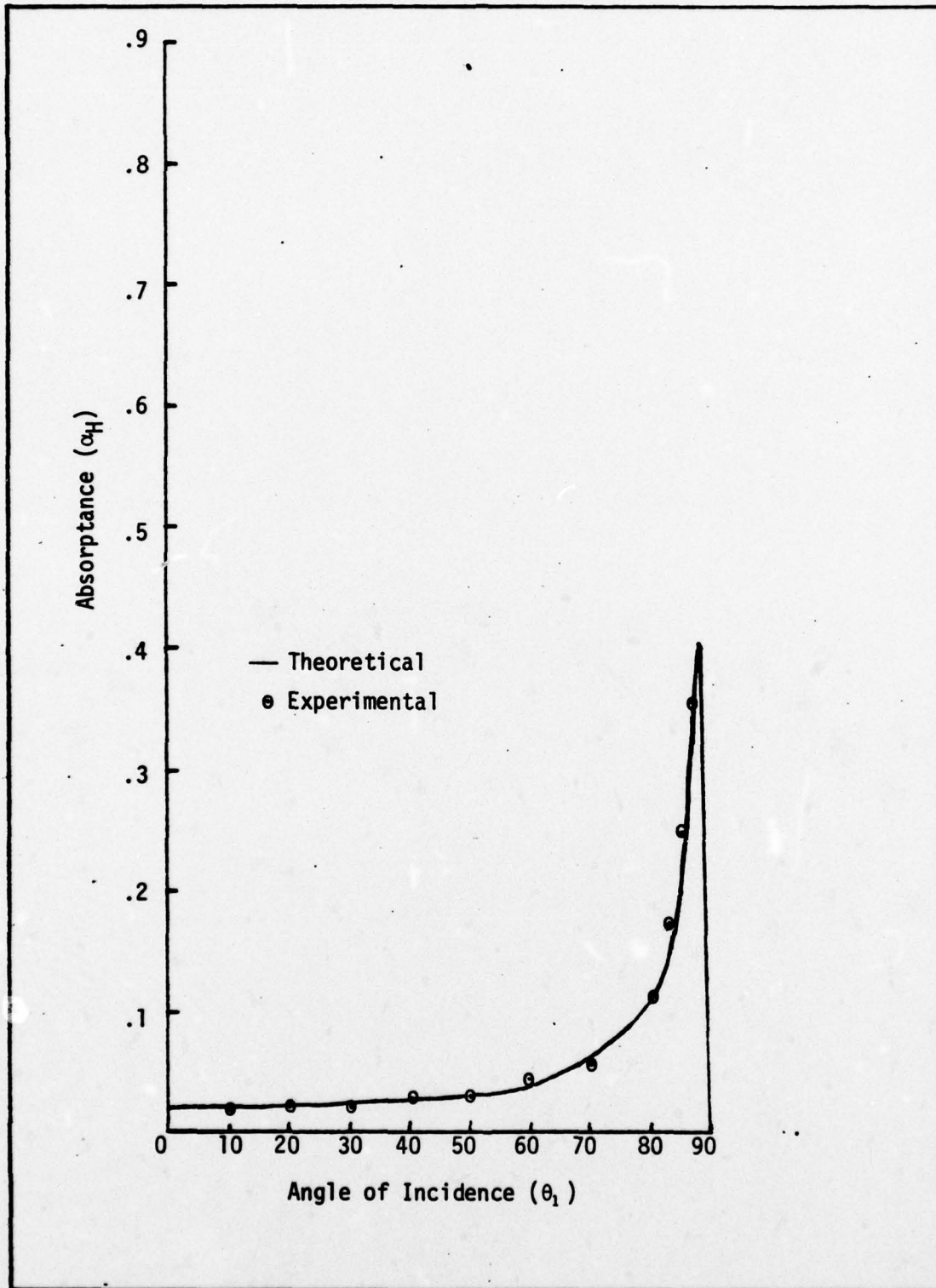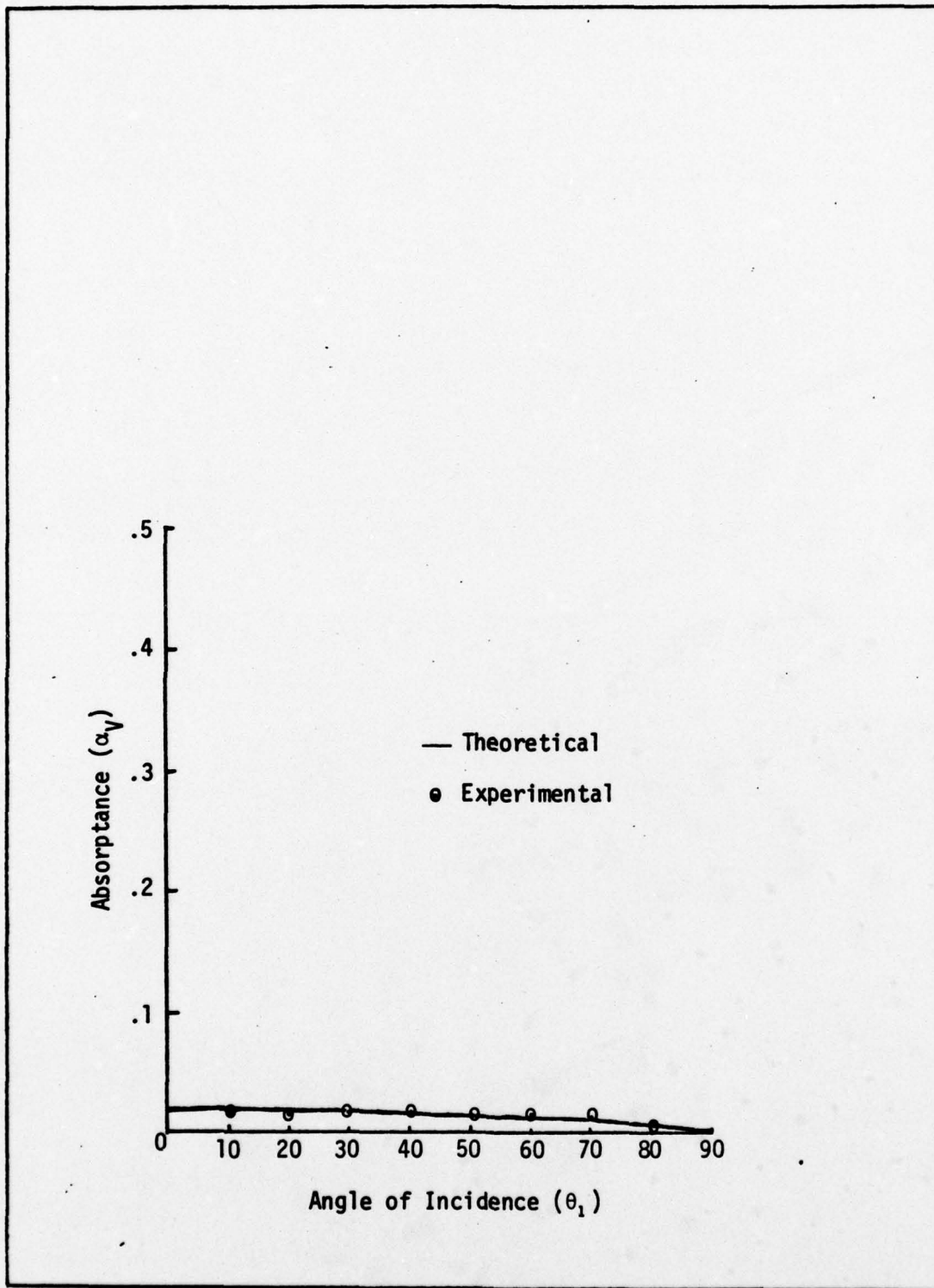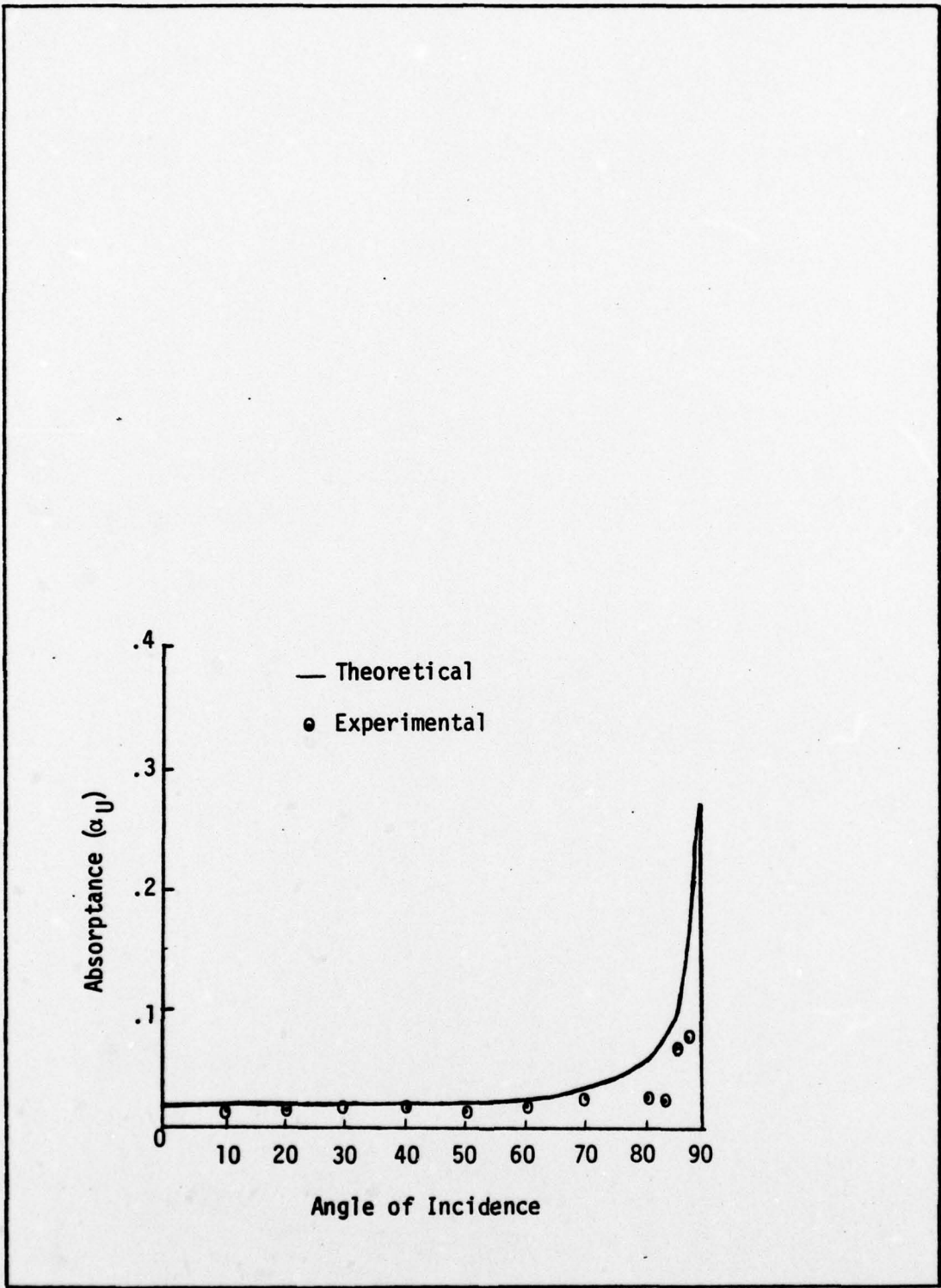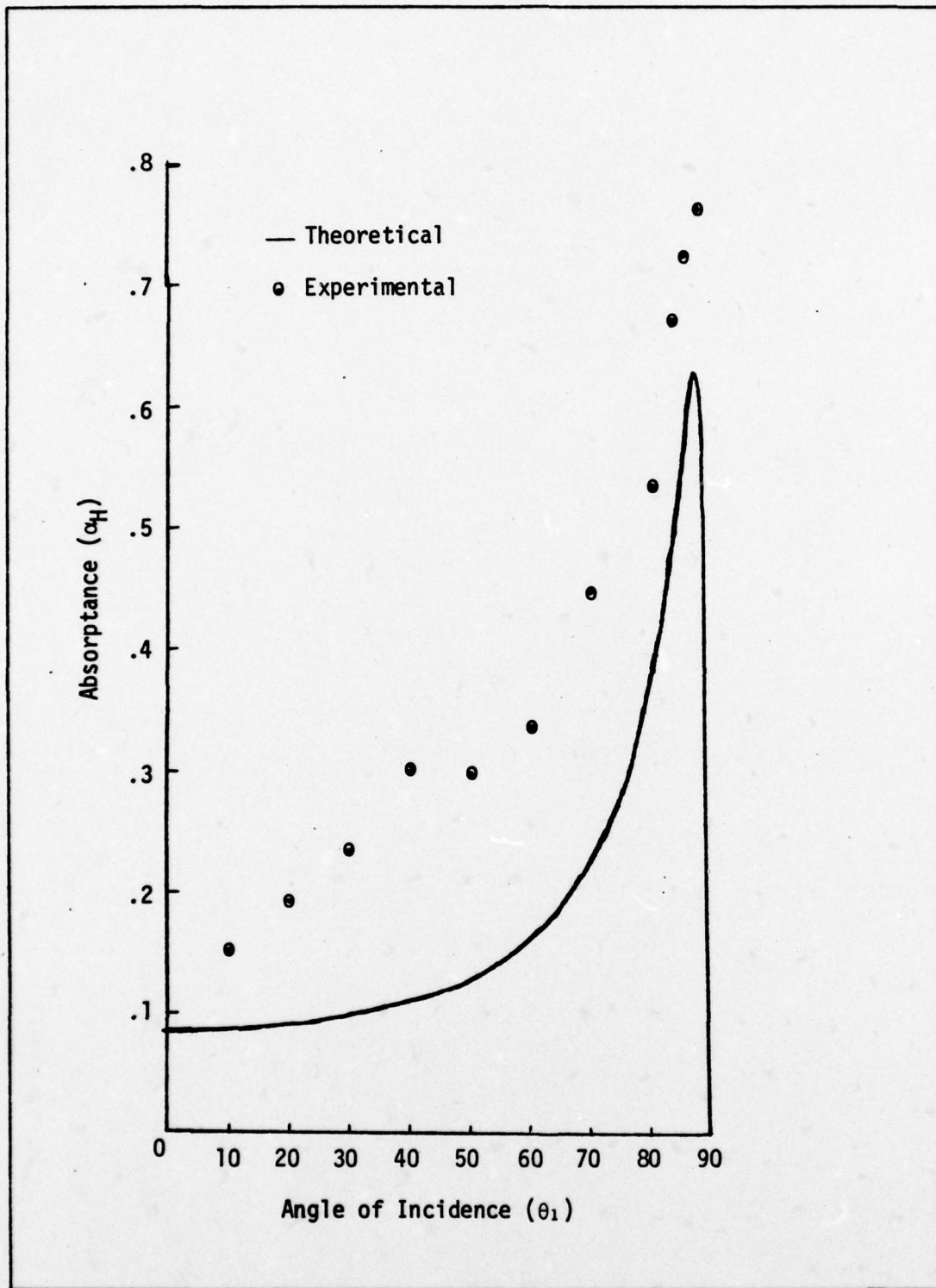Figure 4. Absorptance of Al. Unpolarized.

23

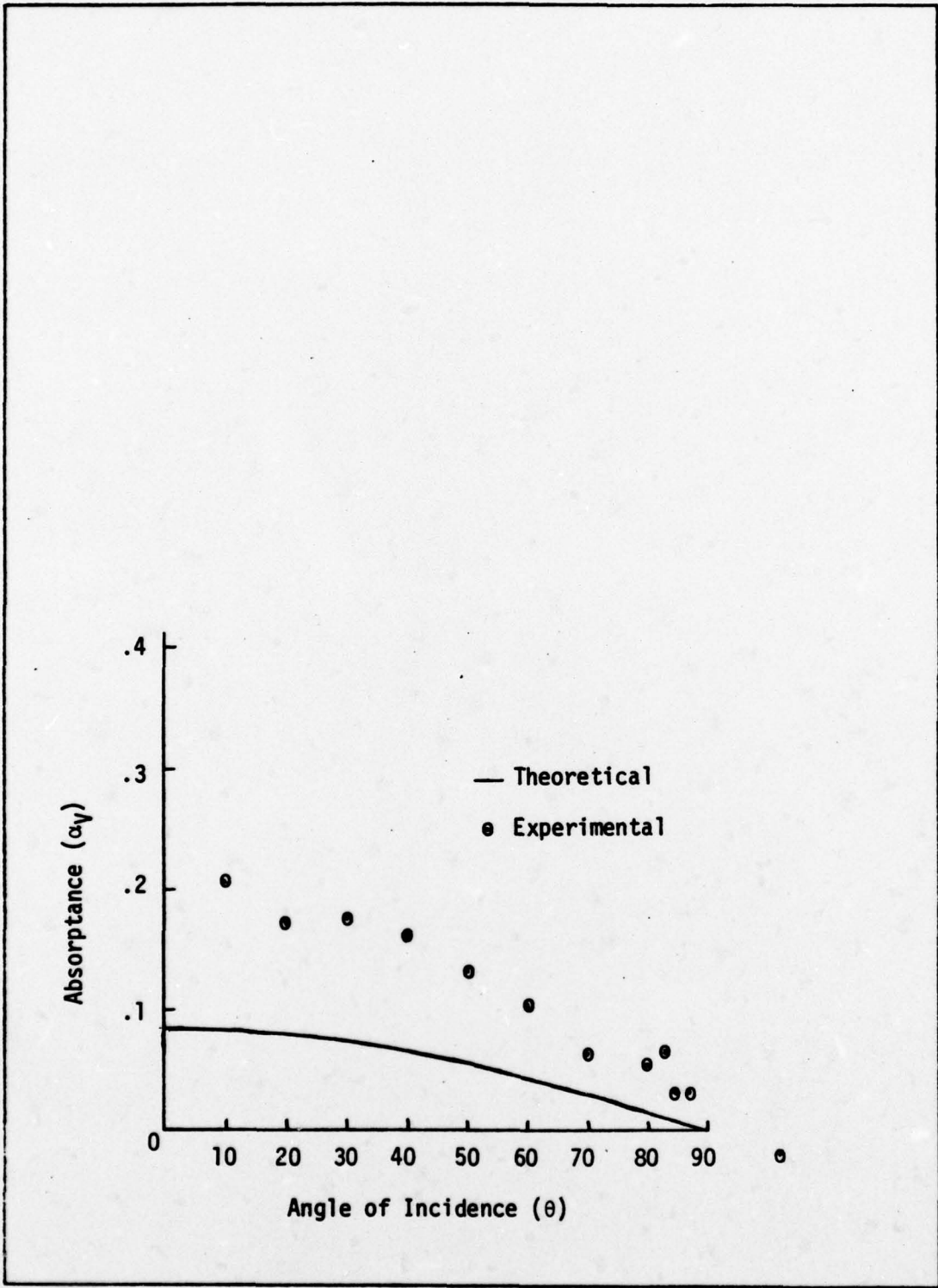Figure 5. Absorptance of Ti. Polarization Parallel to the Plane of Incidence.

24

Figure 6. Absorptance of Ti. Polarization Perpendicular to the Plane of Incidence.

25
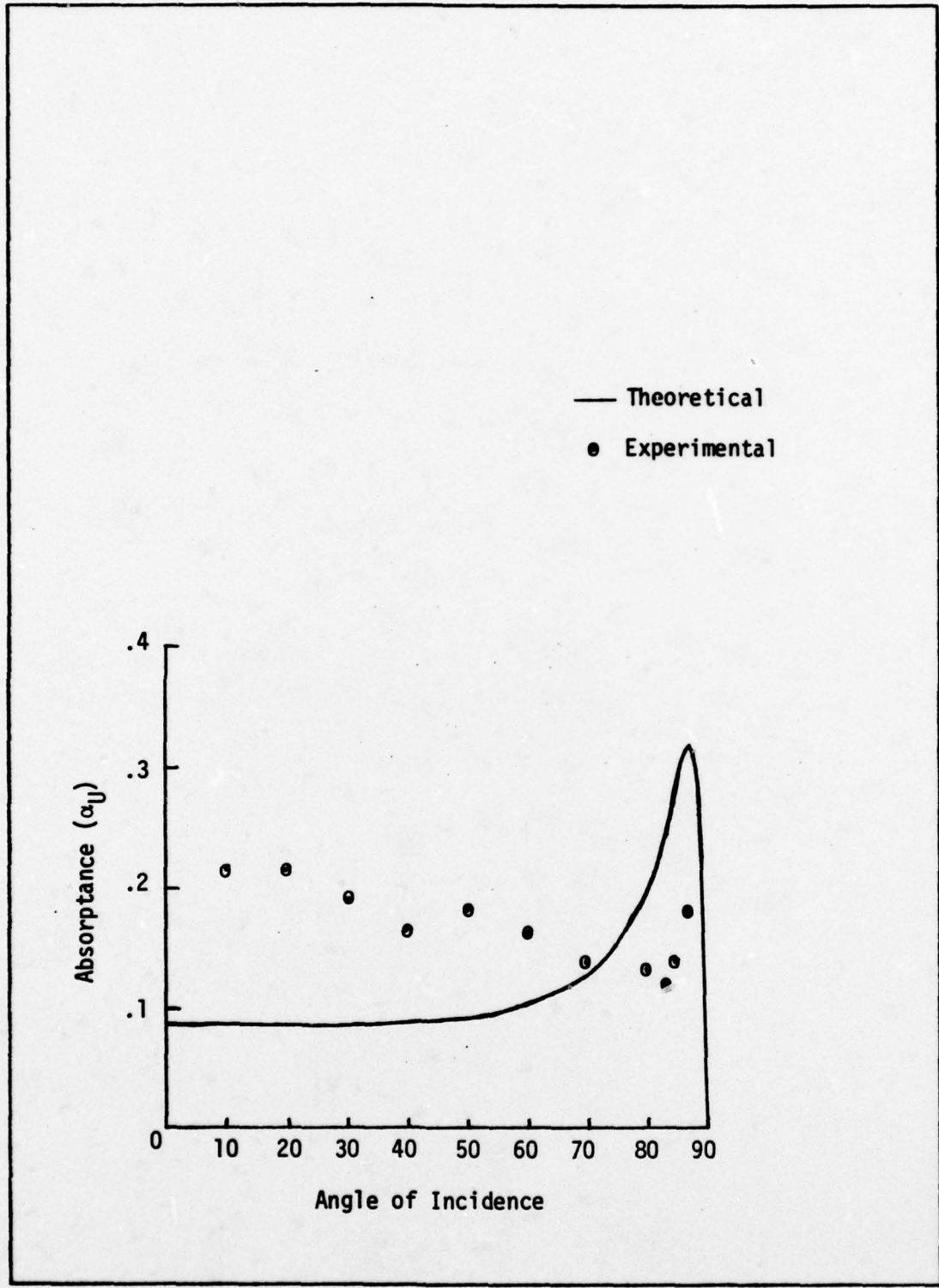
Figure 7. Absorptance of Ti.   Unpolarized.

flat surface, which is not the case for the sanded Cu substrate of Ti. For the roughness rms depth of 0.4 m, the absorptance may increase by 60 percent at $\theta_1 = 10°$ to 15 percent at $\theta_1 = 70°$ (Ref 8: 198). Also, Ti does not build up a protective oxidation layer as does Al. The Ti will continue to oxidize. A 0.07 m layer of oxident will increase the absorptance from 0.086 at $\theta_1 = 25°$ to 0.2 (Ref 8: 198). This is a factor of 2.3 difference and this difference would be greater at higher angles of incidence. For the case of random polarization, the experimental values decrease with increasing θ_1. This is the case if the polarization of the laser is 17 percent perpendicular an and 83 percent parallel.

Error Analysis

A classical approach to error analysis is presented in Appendix F. The purpose of the analysis is to determine which factors contribute the most error. Table V is a comparison of the relative errors for the disc, and samples one, two, three, and five. All the analysis was for Al (α_H) assuming h (free convection coefficient) and ε are in error by 100 percent. It is important to note, the error analysis does not address a breakdown in the isothermal approximation nor any error in θ_1 or the polarization.

TABLE V

Error Analysis Summary

Sample	α_H	$\dfrac{d\alpha_H}{\alpha_H}$	Relative Error Contributions			
			Power	Curve Dependent Values	Free Convection	Radiation
Disc	0.019	0.32	0.07	.08	0.17	0.003
1	0.02	0.14	0.06	.07	0.01	0.001
2	0.04	0.14	0.06	.034	0.04	0.001
3	0.13	0.11	0.06	.03	0.02	0.001
5	0.50	0.17	0.06	.03	0.08	0.001

V. CONCLUSIONS AND RECOMMENDATIONS

Conclusions

This report presents a straightforward experimental approach to determine the absorptance at various angles of incidence and at various polarizations. The experimental values for α_H and α_V agree with the Fresnel equation for smooth surfaces. If one calculates α_U from α_H and α_V, α_U (Al) again agrees with the Fresnel equations. In light of the breakdown in the 50/50 polarization assumption, α_U for Al and Ti are not anticipated to agree with theory. The tests for Ti should have been with a polished sample to facilitate comparison with theory. Two of the samples were slightly smaller than the desired 1.5w which could induce a five percent error in the incident power.

In conclusion, the isothermal approximation is a valid technique for calculating the absorptance. Also, large differences in calculated and theoretical values would be anticipated for the random polarization if the actual polarization favored either parallel or perpendicular. To accurately predict the absorptance of an unpolarized beam, one must insure the surface conditions are smooth, and one must know the degree of polarization of the laser. Fresnel equations do not apply to rough surfaces without a modification.

Recommendations

There are several modifications and improvements which have already been mentioned. The convective term in the heat equation could be decreased by placing a thermal insulator against the back side of the

29

sample. Analysis could be better supported if the power and another thermocouple position could be recorded simultaneously with the primary thermocouple. A third suggestion is to determine the degree of polarization of an unpolarized laser prior to calculating the absorptance. Surface preparation is critical, if the theory is to be applicable to the experiment.

BIBLIOGRAPHY

1. Born, Max and Emil Wolf. <u>Principles of Optics</u> (Fifth Edition). New York: Pergamon Press, 1975.

2. Laughlin, Bill. Air Force Weapons Laboratory (Personal correspondence). Kirtland Air Force Base, New Mexico, 1977.

3. Holland, L. <u>Vacuum Deposition of Thin Films</u>. New York: John Wiley and Sons, Inc., 1958.

4. Carslaw, H. S. and J. C. Jaeger. <u>Condition of Heat in Solids</u> (Second Edition). New York: Oxford University Press, 1959.

5. Hitchcock, James E., Deputy Department Head of Aeronautics and Astronautics, Air Force Institute of Technology (Personal communication). Wright-Patterson Air Force Base, Ohio 1977.

6. Siegman, A. E. <u>An Introduction to Lasers and Masers</u>. New York: McGraw-Hill, Inc., 1971

7. Nielsen, Philip E., Associate Professor of Physics, Air Force Institute of Technology (Personal communication). Wright-Patterson Air Force Base, Ohio, 1977.

8. Edwards, D. K. and Ivan Cotton. "Radiation Characteristics of Rough and Oxidized Metals," <u>Advances in Thermophysical Properties at Extreme Temperatures and Pressures</u> (Third Symposium), editied by S. Gratch. New York: American Society of Mechanical Engineers, 1965.

9. ---. <u>CRC Handbook of Chemistry and Physics</u> (58th Edition), edited by R. C. Weast. Cleveland: CRC Press, 1977.

10. Cox, J. T., et al. "Infrared Reflectance of Silicon Oxide and Magnesium Floride Protected Aluminum Mirrors at Various Angles of Incidence from 8μm to 12μm," <u>Applied Optics</u>, <u>14</u> (<u>6</u>):1247-1250 (June 1975).

11. Harris, L. "Preparation and Infrared Properties of Aluminum Oxide Films," <u>Journal of the Optical Society of America</u>, <u>45</u> (<u>1</u>);27-29 (January 1955).

12. Billings, B. H., et al. <u>American Institute of Physics Handbook</u> (Third Edition). New York: McGraw-Hill, Inc., 1972.

APPENDIX A

Evaporation of Aluminum

APPENDIX A

Evaporation of Aluminum

Prior to evaporation, the Cu substrates were cleaned with a detergent and then rinsed and dried in a denatured alcohol steam bath. From this point, the samples were no longer touched by the hand.

The evaporating apparatus consists of two major systems: the vacuum and the heat source. The vacuum chamber utilizes a standard vacuum pump and a diffusion pump with a capacity to reach 1×10^{-6}mm of Hg. The evaporation is monitored through the chamber walls.

The heating source is a tungsten coil connected to a variable power source (electrical). The power source consists of a variable autotransformer and a stepdown transformer (230v to 7.5v). The current through the coil may be varied from zero to 100 amperes.

First, the Al(99%) wire is melted onto the coil at 5×10^{-6}mm of Hg to boil off any impurities. Approximately 30 amperes of current is required. After the vacuum is released, the Cu is mounted in the chamber approximately seven inches from the coil. During evaporation (5×10^{-6}mm of Hg) the coil is visually monitored through a glass slide approximately seven inches from the coil. When the coil can no longer be seen, the current is turned off and the depth of Al is assumed to be 400Å. The only significance of the depth is that it be greater than the skin depth (100Å).

APPENDIX B

Evaporation of Titanium

APPENDIX B

Evaporation of Titanium

An electron-beam gun heat source is the primary difference between
the evaporation of Al and Ti. The e-gun source and control unit are
made by Varian Vacuum Division (Model 922-0020). The Ti is supported
by an externally controlled sliding tray which facilitates adjustments
during the evaporation process. This method is used to reduce
impurities incurred by the high evaporation temperatures. The skin
depth of Ti is approximately 450Å.

APPENDIX C

Absorptance of Al and Ti as Predicted by Theory

TABLE VI

Theoretical Absorptances

Surface	θ_1	0	10	20	30	40	50	60	70	80	83	85	87	88	89	90
Bare Al	α_H	.02	.02	.02	.023	.026	.03	.036	.06	.106	.148	.198	.299	.39	.531	0
	α_V	.02	.019	.018	.017	.015	.012	.01	.01	.003	.002	0	0	0	0	0
	α_U	.02	.02	.019	.02	.021	.021	.023	.035	.055	.075	.099	.150	.20	.27	0
Al$_2$O$_3$/Al	α_H	.02	.02	.02	.02	.03	.03	.04	.06	.114	.169	.206	.326	.445	.496	0
	α_V	.02	.019	.019	.017	.016	.013	.01	.007	.005	.004	.002	0	0	0	0
	α_U	.02	.02	.02	.019	.023	.022	.025	.034	.06	.087	.104	.163	.223	.248	0
Bare Ti	α_H	.086	.087	.09	.098	.11	.128	.163	.226	.383	.48	.563	.63	.609	.454	0
	α_U	.085	.084	.08	.074	.066	.056	.043	.03	.015	.011	.008	.005	.003	.022	0
	α_V	.086	.085	.086	.086	.088	.092	.103	.128	.199	.246	.286	.318	.306	.228	0

Values for Al$_2$O$_3$ assume n = 1.76 and a thickness of 50A.

37

APPENDIX D

Instrument Calibrations

APPENDIX D

Instrument Calibrations

1. Coherent Radiation Laboratories Model 201 power meter and detector.

    Scale = 30 watt   Output = 0.0347 v/w

2. F. L. Moseley Company Model 7000A x-y Recorder

Scale	Calibration
Y = 0.1 v/in	0.102 v/in
t = 5 v/in	5.02 s/in

3. Keithley Instruments Model 153 Microvolt-Ammeter

Scale	Calibration
1mv	0.921 mv/v
300μv	0.314 mv/v
100μv	0.124 mv/v

APPENDIX E

<u>Properties of Al, Cu, and Ti</u>

APPENDIX E

Properties of Al, Cu, and Ti

A. Specific heats $\left(\frac{cal}{g°C}\right)$ at 25°C   (Ref 9:D-165)

   C(Al) = 0.215

   C(Ti) = 0.125

   C(Cu) = 0.092

B. Densities (g/cm³)

   ρ(Al) = 2.7   (Ref 9:D-171)

   ρ(Ti) = 4.5   (Ref 9:B-171)

   ρ(Cu) = 8.95   (Ref 9:B-216)

C. Emissivities   (Ref 9:E-229)

   ε(Al) = 0.022 at 25°C

   ε(Ti) = 0.05   estimated

   ε(Cu) = 0.02   at 100°C

D. Thermal conductivities $\left(\frac{cal}{s\ cm^2°C}\right)$ at 27°C

   k(Al) = 0.569   (Ref 9:E-10)

   k(Ti) = 0.052   (Ref 9:E-16)

   k(Cu) = 0.957   (Ref 9:E-13)

E. Heat convection ratio $\left(\frac{cal}{s\ cm\ °C}\right)$ (Ref 5:Personal Communication)

   disc   h = 1.36 x 10⁻⁴

   Sample 1   h = 6.8 x 10⁻⁵

   Sample 2   h = 8 x 10⁻⁵

   Sample 3   h = 1 x 10⁻⁴

Sample 4   h = 2.06 x 10^{-4}

Sample 5   h = 2.72 x 10^{-4}

F. Stefan-Boltzman number $\left(\dfrac{cal}{s\ cm^2(°K)^4}\right)$ (Ref 4:21)

$\sigma = 1.37 \times 10^{-12}$

$\sigma_1 = 5.48 \times 10^{-12}$

G. Iron-Constantan thermocouple output

$0.053 \dfrac{mv}{°C}$ (Ref 9:E-110)

H. Index of refraction at λ = 10.6µm

$\tilde{n}(Al) = 28 + 70.4i$ (Ref 10:1247)

$\tilde{n}(Al_2O_3) = 1.76 + 0.1i$

$\tilde{n}(Ti) = 9.5 + 18.3i$ Ref 12:6-152)

42

APPENDIX F

Derivation of Error Analysis

APPENDIX F

Derivation of Error Analysis

The error analysis is derived from a classical mathematical approach. For example, if $\alpha = f(x,y)$, then

$$d\alpha = \frac{\partial f}{\partial x}\, dx + \frac{\partial f}{\partial y}\, dy \qquad (27)$$

or

$$\frac{d\alpha}{\alpha} = \frac{1}{f}\frac{\partial f}{\partial x}\, dx + \frac{1}{f}\frac{\partial f}{\partial y}\, dy \qquad (28)$$

For the isothermal approximation, assuming an Al/Cu sample:

$$\alpha = \frac{1}{P}\left\{\left[(\rho VC)_C + (\rho VC)_A\right]\frac{dT}{dt} + (T-T_a)\left[h(A_C+A_A) + \sigma_1 T_a^3\,(\epsilon_C A_C + \epsilon_A A_A)\right]\right\} \qquad (29)$$

To accommodate an analysis of the individual terms, let

$$\alpha = \frac{B}{P} \qquad (30)$$

$$G = T - T_a \qquad (31)$$

$$Q = \frac{dT}{dt} \qquad (32)$$

$$E = (\rho VC)_C + (\rho VC)_A \qquad (33)$$

$$F = h(A_C+A_A) + \sigma_1 T_a^3\,(\epsilon_C A_C + \epsilon_A A_A) \qquad (34)$$

Therefore,

$$\frac{d\alpha}{\alpha} = \frac{dB}{B} + \frac{dP}{P} \qquad (35)$$

44

The power (P) is a function of two instrument factors and the height of the power curve (ℓ_p) mathematically,

$$P = YM\ell_p \tag{36}$$

where, Y is the recorder calibration and M is the power meter calibration. It follows that

$$\frac{dP}{P} = \frac{dY}{Y} + \frac{dM}{M} + \frac{d\ell_p}{\ell_p} \tag{37}$$

Letting dY = 0.002, Y = 0.1, dM = 0.0005, M = 0.0347, and Dlp = 0.1,

$$\frac{dP}{P} = 0.034 + \frac{0.1}{\ell_p} \tag{38}$$

Utilizing equations 31 - 35, it may be shown:

$$\frac{dB}{B} = \frac{EdQ}{B} + \frac{QdE}{B} + \frac{GdF}{B} + \frac{FdG}{B} \tag{39}$$

Let Q = Js, where J is the calibration of the combined thermocouple, microvoltmeter, and recorder system and s is the net slope (heating plus cooling).
Therefore,

$$dQ = sdJ + Jds \tag{40}$$

From equation (33), it may be shown:

$$dE = (\rho VdC)_C + (\rho CdV)_C + (CVd\rho)_C + (\rho VdC)_A + (\rho CdV)_A + (CVd\rho)_A \tag{41}$$

45

Using equation (34),

$$dF = (A_C + A_A) \, dh + h(dA_C + dA_A) + 3\sigma_1 T_a^2 [\varepsilon_C A_C + \varepsilon_A A_A] \, dT_a$$

$$+ \sigma_1 T_a^3 [\varepsilon_C dA_C + A_C d\varepsilon_C + \varepsilon_A dA_A + A_A d\varepsilon_A] \qquad (42)$$

If ϕ is the temperature conversion factor and β is the maximum height of the temperature curve, then,

$$G = \phi\beta \qquad (43)$$

and

$$dG = \beta d\phi + \phi d\beta \qquad (44)$$

The value for $\frac{d\alpha}{\alpha}$ may be calculated by combining equations (36) and (39) and there subparts.

For a disc,

$$A = \pi r^2 + 2\pi r z \qquad (45)$$

$$V = \pi r^2 z \qquad (46)$$

$$dA = (2\pi r + 2\pi z) \, dr + 2\pi r \, dz \qquad (47)$$

$$dV = 2\pi r z dr + \pi r^2 dz \qquad (48)$$

For an ellipse,

$$p = 4.44 \, (a^2 + b^2)^{\frac{1}{2}} \qquad (49)$$

$$A = \pi a b + p z \qquad (50)$$

$$V = \pi a b z \qquad (51)$$

46

$$dA = \left[\pi b + \frac{4.44za}{(a^2+b^2)^{\frac{1}{2}}}\right] da + \left[\pi a + \frac{4.44zb}{(a^2+b^2)^{\frac{1}{2}}}\right] db + 4.44(a^2+b^2)^{\frac{1}{2}}dz \qquad (52)$$

$$dV = \pi bzda + \pi azdb + \pi abdz \qquad (53)$$

The following values were used in the error analysis calculations:

$$dr_C = dr_A = 0.05cm \text{ (3\% error)}$$

$$dz_C = 0.0005cm \quad (0.6\%)$$

$$dz_A = 200\text{Å} \quad (50\%)$$

$$d\rho_C = d\rho_A = 0.0005 \quad (0.05\%)$$

$$dC_C = dC_A = 0.0005 \quad (0.5\%)$$

$$d\epsilon_C = 0.02 \quad (100\%)$$

$$d\epsilon_A = 0.022 \quad (100\%)$$

The convection coefficient (h) was assumed to be 100 percent in error.
The above values were used regardless of sample size. To evaluate an
entire problem, one must choose a sample and select an experimental graph
to determine the remaining quantities. A typical graph is in Appendix G.
An error analysis summary can be found in Table 5.
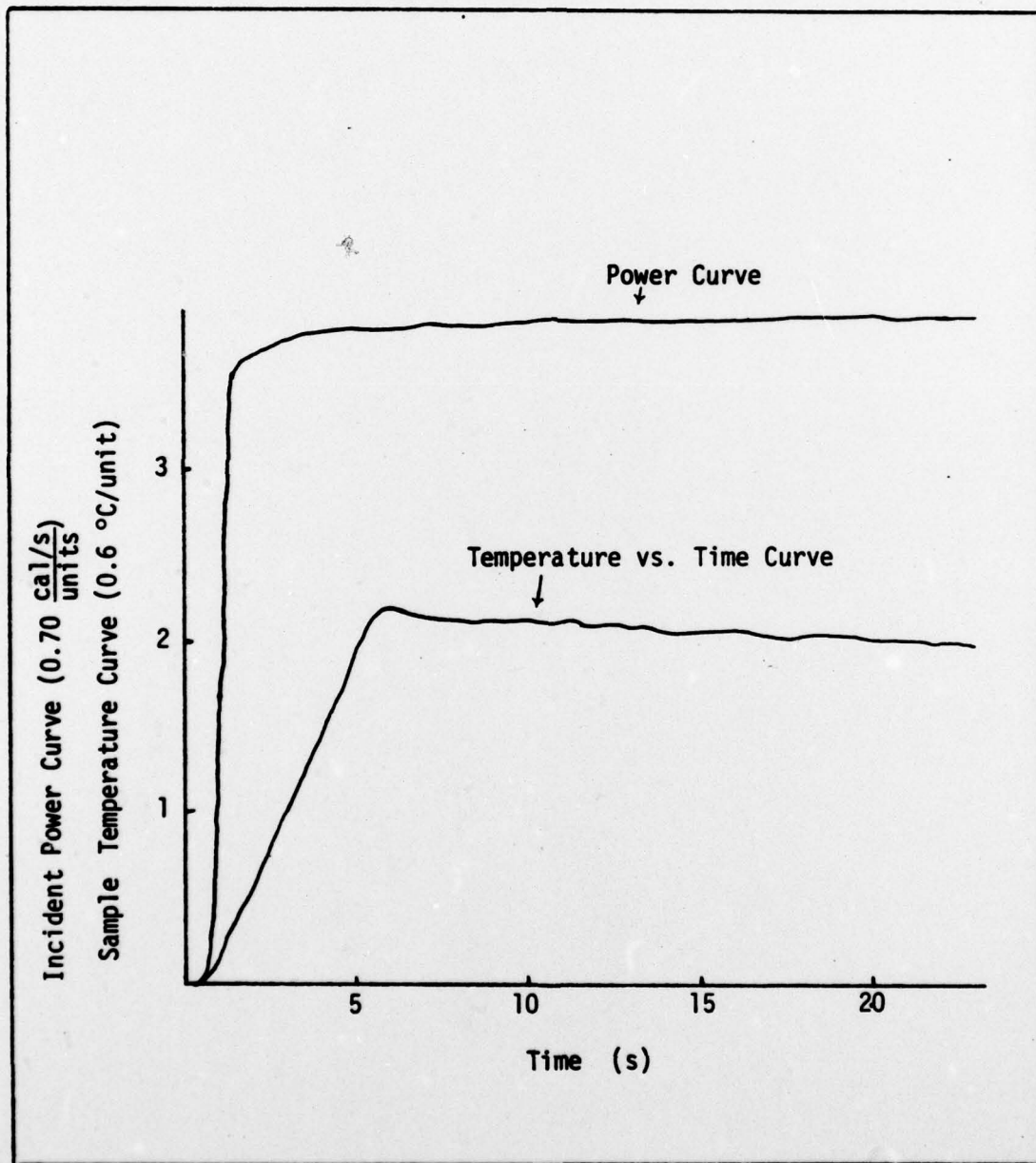
APPENDIX G

Experimental Graph

Figure 8. Experimental graph. α_H; $\theta = 40°$; Al.

49

APPENDIX H

List of the Major Experimental Apparatus

APPENDIX H

List of the Major Experimental Apparatus

1. Coherent Radiation Laboratories Model 201 power meter.

2. Calorimetric power detector (Brand name undetermined).[1]

3. Iron-Constantan thermocouple.

4. Keithley Instruments Model 153 microvolt/ammeter.

5. F. L. Mosley Model 7000A x-y recorder.

6. Spectra Physics Model 132 HeNe laser

7. Coherent Radiation Laboratories Model 42 CO_2 laser with power supply and cooler.

8. Optical benches and associated mounts.

[1]The power meter and detector were calibrated simultaneously.

VITA

Richard Alan Henson was born on October 20, 1948 in Wagoner, Oklahoma. He graduated from Wagoner High School in 1966 and in the Spring of the same year, he entered Northeastern State College in Tahlequah, Oklahoma. Upon graduation from NSC in 1970, he received a Bachelor of Science degree in Physics and Mathematics and in August of 1970, he entered the Air Force Officer Training School and was commissioned on November 18, 1970. Following OTS, he received orders for Undergraduate Pilot Training at Moody Air Force Base, Georgia. After graduation in November of 1971, he completed the water survival school in Florida and the land survival school in Washington. He entered Pilot Instructor Training at Randolph Air Force Base, Texas in February of 1972. His next assignment was to Sheppard Air Force Base in May of 1972 as an instructor pilot in the T-38. After two years, he was assigned to Pilot Instructor Training at Randolph Air Force Base as an instructor until May of 1976. On 1 June 1976 he entered the Air Force Institute of Technology, Dayton, Ohio.

Permanent Address: Rt. 3, Box 321
Wagoner, OK 74467

REPORT DOCUMENTATION PAGE		READ INSTRUCTIONS BEFORE COMPLETING FORM
1. REPORT NUMBER AFIT/GEP/PH/77D-5	**2. GOVT ACCESSION NO.**	**3. RECIPIENT'S CATALOG NUMBER**
4. TITLE (and Subtitle) ABSORPTANCE OF IR LASER RADIATION AT A METALLIC INTERFACE AT VARIOUS ANGLES OF INCIDENCE AND POLARIZATIONS		**5. TYPE OF REPORT & PERIOD COVERED** M.S. Thesis
		6. PERFORMING ORG. REPORT NUMBER
7. AUTHOR(s) Richard A. Henson Captain USAF		**8. CONTRACT OR GRANT NUMBER(s)**
9. PERFORMING ORGANIZATION NAME AND ADDRESS Air Force Institute of Technology (AFIT/EN) Wright-Patterson AFB, OH 45433		**10. PROGRAM ELEMENT, PROJECT, TASK AREA & WORK UNIT NUMBERS**
11. CONTROLLING OFFICE NAME AND ADDRESS Air Force Materials Laboratory Aerospace Research Division Wright-Patterson AFB, OH 45433		**12. REPORT DATE** December 1977
		13. NUMBER OF PAGES 64
14. MONITORING AGENCY NAME & ADDRESS(if different from Controlling Office)		**15. SECURITY CLASS. (of this report)** UNCLASSIFIED
		15a. DECLASSIFICATION/DOWNGRADING SCHEDULE

16. DISTRIBUTION STATEMENT (of this Report)

Approved for public release; distribution unlimited.

17. DISTRIBUTION STATEMENT (of the abstract entered in Block 20, if different from Report)

18. SUPPLEMENTARY NOTES

Approved for public release, IAW
AFR 190-17.

JERRAL F. GUESS, Capt, USAF
Director of Information

19. KEY WORDS (Continue on reverse side if necessary and identify by block number)

Absorption   Calorimeters
Infrared Radiation
Radiation Absorption
Laser Beams

20. ABSTRACT (Continue on reverse side if necessary and identify by block number)

A calorimetric method is developed to measure the absorptance of IR laser radiation at a metallic interface. The absorptance of Al and Ti is measured at various angles of incidence ($10° \div 87°$) and laser polarizations (parallel, perpendicular, and random relative to the plane of incidence). Designing the metal surface to be approximately the size of the beam and using a thin (0.032 in.) sample facilitate the simplifying assumptions. The average incident power is 13 w/cm². For the laser polarizations, parallel and

sq cm

perpendicular, the maximum difference between theoretically and experimentally calculated values is 26 percent and 57 percent respectively for Al and 100 percent and 500 percent respectively for Ti. The Ti values are largely attributed to surface roughness (sanded) and oxidation. Without a Brewster window in the laser cavity, a test revealed the laser polarization was not 50 percent horizontal and 50 percent vertical. The average polarization is 17 percent horizontal and 83 percent vertical.